Synthesis and Characterization of Carbon-Doped TiO_2 Nanostructures with Enhanced Visible Light Response

Guosheng Wu,[†] Tomohiro Nishikawa,[‡] Bunsho Ohtani,[‡] and Aicheng Chen*[,†]

Department of Chemistry, Lakehead University, Thunder Bay, Ontario P7B 5E1, Canada, and Catalysis Research Centre, Hokkaido University, Sapporo 011-0021, Japan

Received May 8, 2007. Revised Manuscript Received July 2, 2007

Carbon-doped TiO_2 micro-/nanospheres and nanotubes have been synthesized via a single source chemical vapor deposition in an inert atmosphere. Organic compound $Ti(OC_4H_9)_4$ was used as the titanium, oxygen, and carbon source, while argon served as the carrier gas. The effect of the temperature, substrate, and the flow rate of the carrier gas is investigated. The diameter of the formed carbon-doped TiO_2 spheres can be adjusted from 100 nm to several micrometers by varying the flow rate of the carrier gas. The as-prepared TiO_2 nanotubes are highly ordered with a diameter of about 100 nm and a wall thickness of around 15 nm. The estimated optical band gap is 2.78 eV for the formed carbon-doped TiO_2 microspheres and 2.72 eV for the synthesized carbon-doped TiO_2 nanotubes, both of which are much smaller than that of bulk anatase TiO_2 (3.20 eV). The photocurrent of the carbon-doped TiO_2 spheres is much higher than that of commercial P-25, which is currently considered as one of the best TiO_2 photocatalysts, especially under visible light irradiation. The possible mechanism of the formation of TiO_2 spheres and nanotubes is also discussed.

Introduction

Nanomaterials and nanostructures are attracting tremendous attention in both fundamental studies and applications due to their unique physical and chemical properties. Of the various types of nanostructured materials, titania (TiO_2) nanostructures are extensively studied because of their broad range of applications.[1,2] TiO_2 photocatalysis provides promising technologies for environmental purification, chemical synthesis, energy renewal, and energy storage due to its strong oxidizing power of photogenerated holes, its chemical inertness, and nontoxicity.[3] While notable advances have been made over the past two decades, three challenges still remain: (i) to increase the quantum yields, which is defined as the number of reaction events occurring per photon absorbed; (ii) to improve the reaction selectively to produce desired chemical synthesis products; and (iii) to shift the irradiation light from UV to visible light as UV light accounts for only a small portion of solar energy compared to visible light. To address those challenges, lately considerable attention has been focused on fabricating different TiO_2 nanostructures (nanoparticles, nanowires, nanotubes, etc.).[4−10] TiO_2 nanoparticles have been fabricated by various methods including sol−gel, hydrothermal method, and coprecipitation.[11−13] Most methods mentioned above require multiple steps to obtain monodispersed particles. Meanwhile, several approaches have also been reported for synthesis of one-dimensional TiO_2 nanostructures, for instance, electrochemical anodization of Ti in aqueous F-containing electrolytes,[14−16] seeded growth,[7] hydrothermal processes,[17−19] sol−gel transcription using organogelators as templates,[20−21] and chemical vapor deposition (CVD).[22]

* Corresponding author Tel: 807-3438318. Fax: 807-3467775. E-mail: aicheng.chen@lakeheadu.ca.

[†] Lakehead University.

[‡] Hokkaido University.

(1) (a) Iijima, S. *Nature* **1991**, *354*, 56. (b) Bavykin, D. V.; Friedrich, J. M.; Walsh, F. C. *Adv. Mater.* **2006**, *18*, 2807.

(2) (a) Peng, X.; Chen, A. *Adv. Funct. Mater.* **2006**, *16*, 1355. (b) Liu, S.; Chen, A. *Langmuir* **2005**, *21*, 8409. (c) Palmisano, G.; Addamo, M.; Augugliaro, M. V.; Caronna, T.; García-López, E.; Loddo V.; Palmisano, L. *Chem. Commun.* **2006**, *9*, 1012.

(3) (a) Heller, A. *Acc. Chem. Res.* **1995**, *28*, 503. (b) Ohtani, B.; Iwai, K.; Nishimoto, S.; Sato, S. *J. Phys. Chem.* **1997**, *101*, 3349. (c) Moriguchi, I.; Hidaka, R.; Yamada, H.; Kudo, T.; Murakami, H.; Nakashima, N. *Adv. Mater.* **2006**, *18*, 69. (d) Wang, C. Y.; Groenzin, H.; Shultz, M. J. *J. Am. Chem. Soc.* **2005**, *127*, 9736.

(4) Chae, W. S.; Lee, S. W.; Kim, Y. R. *Chem. Mater.* **2005**, *17*, 3072.

(5) Jun, Y. W.; Casula, M. F.; Sim, J. H.; Kim, S. Y.; Cheon, J.; Alivisatos, A. P. *J. Am. Chem. Soc.* **2003**, *125*, 15981.

(6) Kasuga, T.; Hiramatsu, M.; Hoson, A.; Sekino, T.; Niihara, K. *Adv. Mater.* **1999**, *11*, 1307.

(7) Tian, Z. R.; Voigt, J. A.; Liu, J.; Mckenzie, B.; Xu, H. F. *J. Am. Chem. Soc.* **2003**, *125*, 12384.

(8) Beranek, R.; Tsuchiya, H.; Sugishima, T.; Macak, J. M.; Taveira, L.; Fujimoto, S.; Kisch, H.; Schmuki, P. *Appl. Phys. Lett.* **2005**, *87*, 243114.

(9) Lin, Y.; Wu, G. S.; Yuan, X. Y.; Xie, T.; Zhang, L. D. *J. Phys.: Condens. Matter* **2003**, *15*, 2917.

(10) Kartini, I.; Meredith, P.; Zhao, X. S.; Diniz da Costa, J. C.; Lu, G. Q. *J. Nanosci. Nanotech.* **2004**, *4*, 270.

(11) Zhang, Z.; Wang, C. C.; Zakaria, R.; Ying, J. Y. *J. Phys. Chem. B* **1998**, *102*, 10871.

(12) Cheng, H.; Ma, J.; Zhao, Z.; Qi, L. M. *Chem. Mater.* **1995**, *7*, 663.

(13) Palmisano, L.; Augugliaro, V.; Sclafani, A.; Schiavello, M. *J. Phys. Chem.* **1988**, *92*, 6710.

(14) Park, J. H.; Kim, S.; Bard, A. J. *Nano. Lett.* **2006**, *6*, 24.

(15) (a) Mor, G. K.; Varghese, O. K.; Paulose, M.; Grimes, C. A. *Adv. Funct. Mater.* **2005**, *15*, 1291. (b) Mor, G. K.; Shankar, K.; Paulose, M.; Varghese, O. K.; Grimes, C. A. *Nano Lett.* **2006**, *6*, 215.

(16) (a) Macak, J. M.; Tsuchiya, H.; Schmuki, P. *Angew. Chem., Int. Ed.* **2005**, *44*, 2100. (b) Beranek, R.; Tsuchiya, H.; Sugishima, T.; Macak, J. M.; Taverira, L.; Fujimoto, S.; Kisch, H.; Schmuki, P. *Appl. Phys. Lett.* **2005**, *87*, 243114.

(17) Kasuga, T.; Hiramatsu, M.; Hoson, A.; Sekino, T.; Niihara, K. *Langmuir* **1998**, *14*, 3160.

(18) Chen, Q.; Zhou, W. Z.; Du, G. H.; Peng, L. H. *Adv. Mater.* **2002**, *14*, 1208.

(19) Yao, B. D.; Chan, Y. F.; Zhang, X. Y.; Zhang, W. F.; Yang, Z. Y.; Wang, N. *Appl. Phys. Lett.* **2003**, *82*, 281.

10.1021/cm071244m CCC: $37.00
Published on Web 08/15/2007

The fundamental aspects of CVD (e.g., process principal, deposition mechanism, reaction chemistry, thermodynamics, kinetics), the advantages, and limitations of CVD as well as its applications have been reviewed recently by Choy.[23] CVD is a relatively mature and useful technique to synthesize TiO_2 thin films and nanomaterials.[24−30] The size distribution can be controlled by adjusting the temperature of the substrate. Precursors used in CVD can be gases, liquids, or solids. Important factors in considering compounds for use as precursors in CVD have been reviewed by O'Brien and coworkers.[31] The delivery of liquid precursors has been dominated by the use of so-called "bubblers", and an ideal liquid precursor should possess a significant vapor pressure. For instance, inorganic Ti precursors with low boiling points (e.g., $TiCl_4$) are introduced into a CVD reactor with a carrier gas to produce TiO_2 films.[32−33] Most organic Ti precursors, such as titanium isopropoxide, have very low vapor pressure, requiring heating to increase the equilibrium vapor pressure within the bubbler. However, two potential problems are associated with this technique. First, to prevent condensation of the precursor in other parts of the CVD system, it may become necessary to heat the entire network of feed lines upstream of the substrate. Second, for delivery to be successful, the precursors must have long-term stability at the elevated temperature used. In this study, titanium(IV) n-butoxide ($Ti(OC_4H_9)_4$) was chosen, for the first time, as a Ti precursor to synthesize TiO_2 nanomaterials. Titanium-(IV) n-butoxide is inexpensive, commercially available, and stable. It is liquid at room temperature with a very high boiling point, 312 °C. In order to circumvent the heating difficulties associated with a liquid precursor with a very low vapor pressure we put the precursor $Ti(OC_4H_9)_4$ inside the CVD reactor. This makes the CVD operation much simpler and more convenient for the mass production of TiO_2 nanomaterials.

In addition, it is well-known that crystalline TiO_2 exhibits effective photocatalysis, while amorphous TiO_2 does not.[34] Many synthesis techniques have been developed to synthesize TiO_2 particles, although there are still difficulties in the production of high-quality spherical crystalline TiO_2 particles. In industrial production, TiO_2 particles are produced based on the so-called "sulfate" and "chloride" processes.[35] TiO_2 particles produced by these methods are usually not in spherical shapes. Recently, hydrothermal methods have been proposed to synthesize spherical TiO_2.[11] However, the as-synthesized particles are usually amorphous or poorly crystallized due to low synthesis temperature.[36]

Recent studies reveal that doping C, N, F, or S enhances the photocatalytic activity of TiO_2.[37−43] Although carbon-doped TiO_2 thin film can be fabricated using the flame oxidation of Ti metal, rutile is the dominant phase, and it is difficult to control the morphology of the formed TiO_2 film.[39] In this paper, we present a facile and reproducible technique to synthesize, on a large scale, carbon-doped TiO_2 spheres formed on Ti substrates and carbon-doped TiO_2 nanotubes within nanochannels of alumina template using CVD. The effect of temperature and flow rate of the carrier gas was studied. The as-synthesized carbon-doped TiO_2 nanostructures and microstructures were characterized using scanning electron microscopy and X-ray diffraction. Our study demonstrates that the Ti precursor, $Ti(OC_4H_9)_4$, can effectively provide sources of titanium, carbon, and oxygen to form carbon-doped TiO_2 nanostructures with enhanced visible light response.

Experimental Section

Titanium plates of 1.0 × 12.5 × 8 mm were degreased first using acetone, then washed with distilled water, etched in 18% HCl at 85 °C for 15 min, then completely washed with distilled water, and finally dried in a vacuum oven at 40 °C. For comparison, silicon, aluminum, and glassy carbon plates were also used as the substrates. All experiments were carried out in a horizontal tube furnace equipped with a quartz tube (diameter 35 mm, length 700 mm). To fabricate TiO_2 spheres, the pretreated Ti plates and the other substrates (e.g., Si, Al) were placed into the center of the quartz tube, and a ceramic boat loaded with $Ti(OC_4H_9)_4$ was placed on the upper stream of argon flow (∼10 cm away from the Ti plates). To synthesize TiO_2 nanotubes, the Ti precursor $Ti(OC_4H_9)_4$ was loaded into a ceramic boat and covered with a porous anodic alumina (PAA) template. Then the boat was placed in the middle of the quartz tube. Prior to heating, the system was purged using ultrapure argon (99.9995%) at a flow rate of 200 standard cubic cm per min (sccm) for 4 h, then the system was heated to a predetermined temperature, the temperature was maintained for 2 h, and then the system was cooled to room temperature with a continuous purge of the pure argon stream. Finally, the synthesized TiO_2 was annealed in air at 500 °C for 1 h.

The PAA templates used in this work were prepared by a two-step aluminum anodic oxidation process in a 0.3 M oxalic acid

(20) Jung, J. H.; Kobayashi, H.; van Bommel, K. J. C.; Shinkai, S.; Shimizu, T. *Chem. Mater*. **2002**, *14*, 1445.
(21) Kobayashi, S.; Hamasaki, N.; Suzuki, M.; Kimura, M.; Shirai, H.; Hanabusa, K. *J. Am. Chem. Soc.* **2002**, *124*, 6550.
(22) Peng, X.; Wang, J.; Thomas, D. F.; Chen, A. *Nanotechnology* **2005**, *16*, 2389.
(23) Choy, K. L. *Prog. Mater. Sci.* **2003**, *48*, 57.
(24) Chen, X. B.; Mao, S. S. *J. Nanosci. Nanotechnol*. **2006**, *6*, 906.
(25) Evans, P.; Pemble, M. E.; Sheel, D. W. *Chem. Mater*. **2006**, *18*, 5750.
(26) Apatiga, L. M.; Rivera, E.; Castano, V. M. J. *Am. Ceram. Soc*. **2007**, 932.
(27) Yang, W. L.; Wolden, C. A. *Thin Solid Films* **2006**, *515*, 1708.
(28) Mellott, N. P.; Durucan, C.; Pantano, C. G.; Guglielmi, M. *Thin Solid Films* **2006**, *502*, 112.
(29) Peng, X.; Chen, A. *J. Mater. Chem.* **2004**, *14*, 2542.
(30) Mathur, S.; Kuhn, P. *Surf. Coat. Technol*. **2006**, *201*, 807.
(31) O'Brien, P.; Pickett, N. L.; Otway, D. J. *Chem. Vap. Deposition* **2002**, *8*, 237.
(32) O'Neill, S. A.; Parkin, I. P.; Clark, R. J. H.; Mills, A.; Elliot, N. *J. Mater. Chem*. **2003**, *13*, 56.
(33) Hyett, G.; Green, M.; Parkin, I. P. *J. Am. Chem. Soc.* **2006**, *128*, 12147.
(34) Ohtani, B.; Ogawa, Y.; Nishimoto, S. I. *J. Phys. Chem*. **1997**, *B101*, 3746.
(35) *Kirk-Othmer Encyclopedia of Chemical Technology*; Howe-Grant, M., Ed.; John Wiley & Sons, Inc.: 1997; Vol. 24, p 225.
(36) Zhang, Y. X.; Li, G. H.; Wu, Y. C.; Luo, Y. Y.; Zhang, L. D. *J. Phys. Chem. B* **2005**, *109*, 5481.
(37) Lakshmi, B. B.; Dorhout, P. K.; Martin, C. R. *Chem. Mater*. **1997**, *9*, 857.
(38) Asahi, R.; Morikawa, T.; Ohwaki, T.; Aoki, K.; Taga, Y. *Science* **2001**, *293*, 269.
(39) Kahn, S. U. M.; Al-Shahry, M.; Ingler, W. B., Jr. *Science* **2002**, *297*, 2243.
(40) In, S.; Orlov, A.; Garcia, F.; Tikhov, M.; Wright, D. S.; Lambert, R. M. *Chem. Commun*. **2006**, *40*, 4236.
(41) Ho, W.; Yu, J. C.; Lee, S. *Chem. Commun.* **2006**, *10*, 1115.
(42) Hahn, R.; Ghicov, A.; Salonen, J.; Lehto, V. P.; Schmuki, P. *Nanotechnology* **2007**, *18*, 105604.
(43) Ghicov, A.; Macak, J. M.; Tsuchiya, H.; Kunze, J.; Haeublein, V.; Frey, L.; Schmuki, P. *Nano Lett.* **2006**, *6*, 1080.

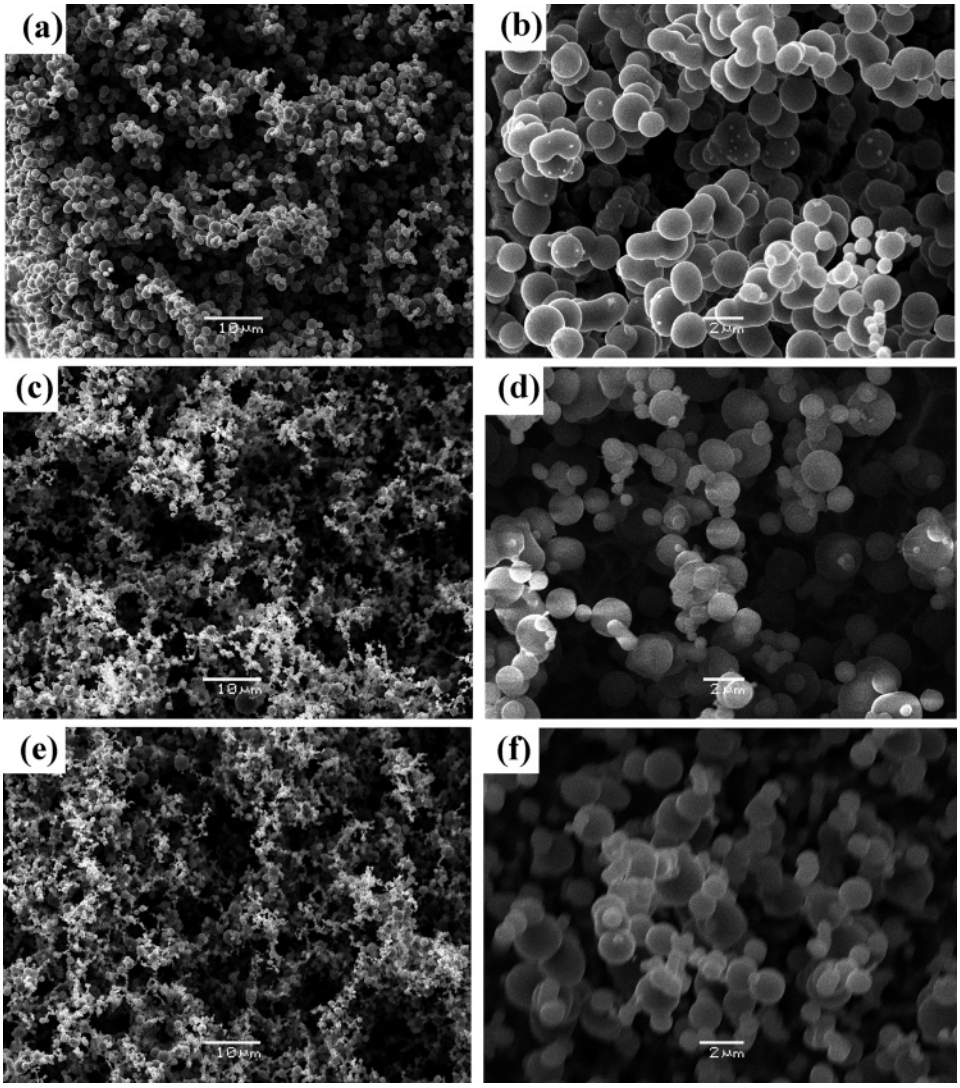

Figure 1. Low and high magnification SEM images of TiO_2 spheres prepared at (a and b) 500 °C; (c and d) 650 °C; and (e and f) 750 °C.

solution.[44] Briefly, after being annealed in a vacuum (773 K) and degreased in acetone, highly pure Al plate (99.999%) was anodized in 0.3 M oxalic acid solution at a constant potential of 40 V for 8 h. After removal of the anodic oxide layer in a mixture of phosphoric acid and chromic acid solution, the textured Al plate was anodized again under the same conditions as the first anodization. Then the Al layer of the sample was removed in a saturated $SnCl_4$ solution. After the coating layer was dissolved in acetone, the barrier layer of the membrane was removed in phosphoric acid to form a regular hollow membrane.

The synthesized TiO_2 spheres and nanotubes were characterized by X-ray diffraction (XRD) (Philips PW 1050-3710 diffractometer with Cu Kα radiation), scanning electron microscopy (SEM) (JEOL JSM 5900LV) equipped with an energy dispersive X-ray spectrometer (EDS) (Oxford Links ISIS), transmission electron microscopy (TEM) (JEOL 2010F) and UV−vis spectroscopy (Varian Cary 5E). To determine the relative concentration of carbon in samples, the EDS analysis was calibrated with a standard SiC sample. Photoelectrochemical experiments were carried out in a glass cell using a three-electrode system controlled by a VoltaLab 40 potentiostat (PGZ 301, Radiometer analytical). The electrolyte used in this study was 0.5 M Na_2SO_4. A Pt coil was used as the counter electrode and was flame annealed before each experiment. A saturated Ag/AgCl electrode was used the reference electrode. The synthesized TiO_2 spheres were used as the working electrode. The UV source was Cure Spot 50 (ADAC systems). The wavelength range was from 280 to 450 nm, and the light intensity was 2 mW/cm^2. For visible light irradiance, the light from the source was passed through an optical filter, which cut off wavelengths below 420 nm. The intensity of the resulting visible light was ~0.015 mW/cm^2. P-25 was used as the benchmark to evaluate the photoelectrochemical activity of the synthesized TiO_2 spheres. P-25 is a mixture of anatase (~79%) and rutile (~21%) TiO_2, and it is currently considered as one of the best commercial TiO_2 photocatalysts. For SEM observation of the formed TiO_2 nanotubes the alumina template was partially dissolved in 2 M NaOH. The template was completely dissolved in 2 M NaOH, and the individual TiO_2 nanotubes were dispersed in ethanol for TEM characterization.

Results and Discussion

Effect of Temperature on the Morphology of the Formed TiO_2 Spheres. Figure 1 presents the low and high magnification SEM images of the samples synthesized at 500 °C (a and b), 650 °C (c and d), and 750 °C (e and f) using $Ti(OC_4H_9)_4$ as the starting material at an argon flow rate of 100 (sccm). As shown in the low magnification SEM images (a, c, and e), all samples possess a porous network

(44) (a) Son, S. J.; Reichel, J.; He, B.; Schuchman, M.; Lee, S. B. *J. Am. Chem. Soc*. 2005, *127*, 7316. (b) Peng, X.; Chen, A. *Nanotechnology* **2004**, *15*, 743.

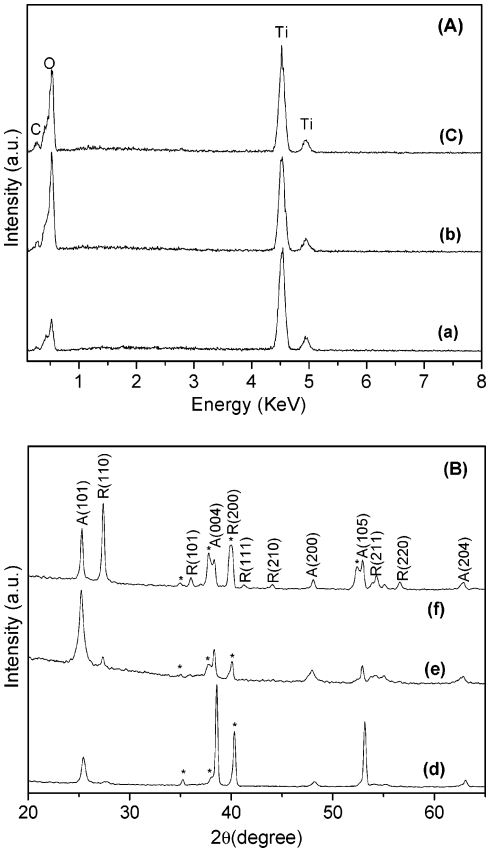

Figure 2. A: EDS of the samples prepared at (a) 500 °C; (b) 650 °C; and (c) 750 °C. B: XRD patterns of the samples synthesized at (d) 500 °C; (e) 650 °C; and (f) 750 °C.

structure formed by a huge number of small spheres. Their corresponding high magnification SEM images (b, d, and f) reveal that the diameters of the formed spheres are within 2 μm and that the morphology of the microspheres synthesized at the different temperatures is very similar. We further investigated the composition of the formed microspheres using EDS. Strong Ti and O peaks are seen in Figure 2A with a ratio close to 1:2, indicating the formed microspheres are TiO_2. In addition, a small carbon peak (~3%) appears in the three EDS spectra. The corresponding XRD patterns of the three samples synthesized at 500, 650, and 750 °C are presented in Figure 2B. The peaks marked by a star are derived from the Ti substrate. Only anatase phase TiO_2 can be seen in the samples prepared at 500 °C (Figure 2d). In contrast, with the increase of temperature, rutile phase TiO_2 appeares gradually, both anatase and rutile coexist in the samples produced at 650 °C (Figure 2e), and the rutile phase becomes the dominant phase at 750 °C (Figure 2f).

Effect of the Flow Rate of the Carrier Gas on the TiO_2 Spheres. To study the impact of the carrier gas flow rate on the formation of the TiO_2 spheres, we chose two different flow rates, 100 and 200 sccm, while the temperature was kept at 500 °C. As shown in Figure 3a, the diameter of the formed spheres is around 2 μm at a flow rate of 100 sccm, consistent with the observation shown in Figure 1b. The diameter of the formed spheres became much smaller, ~100 nm, when we increased the flow rate to 200 sccm (Figure 3b); the coverage of the formed nanospheres is lower than

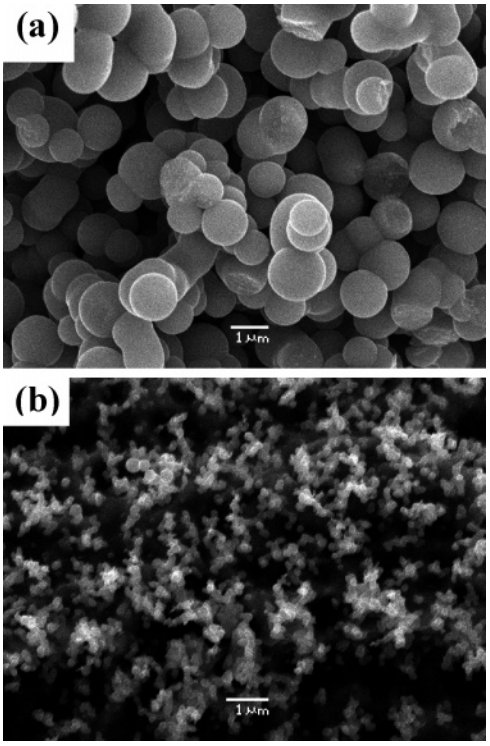

Figure 3. SEM images of TiO_2 spheres prepared under 500 °C at the Ar flow rate of (a) 100 sccm and (b) 200 sccm.

that of the formed microspheres due to the increase of the Ar flow rate.

Effect of Substrates on the Formation of TiO_2 Spheres. For comparison, silicon, aluminum, and glassy carbon plates were also used as the substrate. As shown in Figure 4, very similar porous network structures composed of a huge number of microspheres were formed on the Ti, Al, Si, and glassy carbon plates (Figure 4 (parts a, b, c, and d, respectively)) at 500 °C and the flow rate of 100 sccm. The diameters of these spheres are all about 2 μm. We further investigated the initial stage of the formation of the TiO_2 microspheres. The CVD experiments on the four different substrates, Ti, Al, Si and glassy carbon plates, were carried out under the same conditions as described above except that the reaction time was 10 min instead of 2 h. Their SEM images reveal that the TiO_2 nanoparticles and nanospheres formed on the four different substrates are very similar. All the above results show that there is no obvious influence of the substrate on the morphologies and compositions of the formed TiO_2 spheres.

The Formation of Carbon-Doped TiO_2 Nanotubes. As the substrates have no obvious influence on the formation of the TiO_2 spheres, it is expected that different TiO_2 nanostuctures can be formed using different templates. In this study, alumina templates were fabricated and used to synthesize TiO_2 nanotubes. Figure 5a presents an SEM image of the porous alumina template; the diameter of the pore is around 100 nm. To synthesize TiO_2 nanostructures, we placed the template on a ceramic boat containing the organic Ti precursor $Ti(OC_4H_9)_4$ and increased the temperature to 500 °C. As shown in Figure 5b, well-aligned nanotubes were formed. The diameter of the nanotubes is around 100 nm, and the wall thickness of is approximately 15 nm. Figure 5c

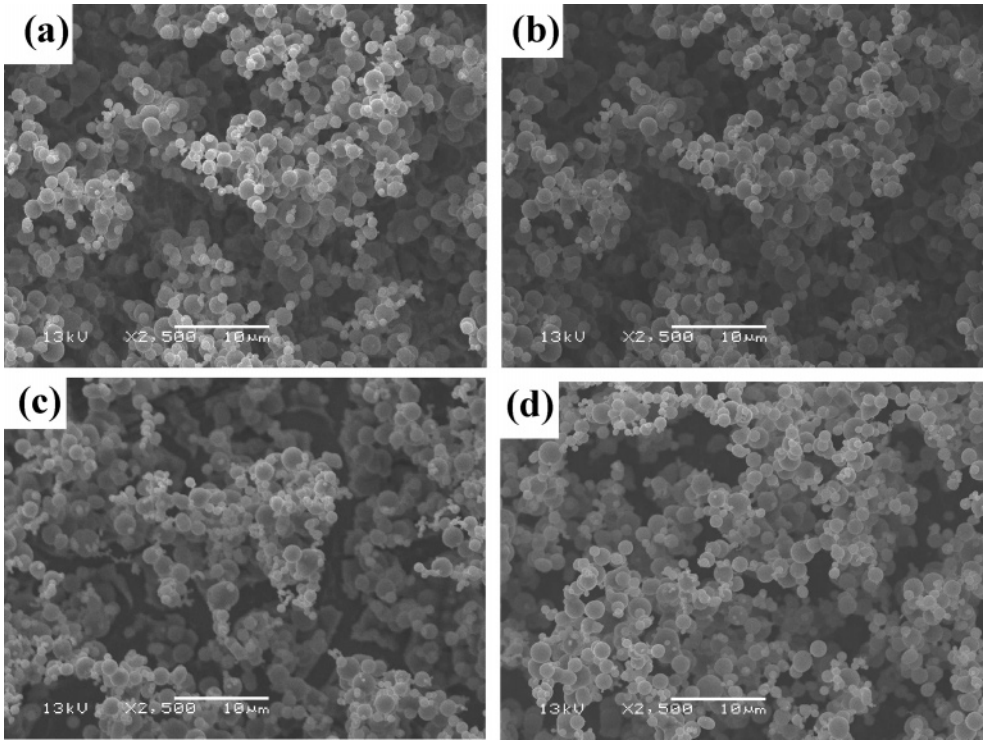

Figure 4. SEM images of TiO_2 spheres synthesized on substrates of (a) Ti; (b) Al; (c) Si; and (d) glassy carbon at 500 °C. The Ar flow rate was 100 sccm.

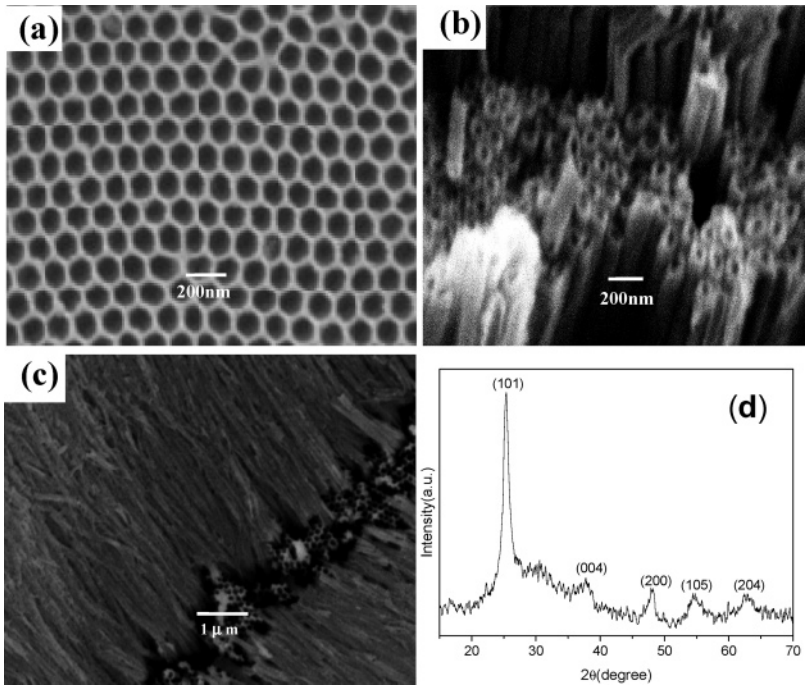

Figure 5. SEM images of (a) the porous alumina template; (b) the top-view of the TiO_2 nanotubes synthesized from $Ti(OC_4H_9)_4$ at 500 °C; (c) the cross section view of a TiO_2 nanotube; and (d) the XRD pattern of the formed TiO_2 nanotubes.

shows the cross section SEM image of the nanotubes imbedded in the template. Their crystallographic characterization was performed using XRD. Peaks observed in Figure 5d equal to 25.6, 38.1, 48.2, and 54.7° correspond to an anatase structure (JCPDS 21-1272), showing that anatase TiO_2 nanotubes were formed. The TEM image of a synthesized TiO_2 nanotube is presented in Figure 6a, further showing that the diameters of the TiO_2 nanotubes are around 100 nm and the wall thickness is approximately 15 nm. Figure 6b presents the selected area electron diffraction (SAED) from the nanotube. The presence of the ring patterns reveals the formation of polycrystalline TiO_2 nanotubes. Meanwhile, the SAED pattern shows (101), (004), (200), and (105) diffractions of the anatase phase, which is consistent with the XRD result shown in Figure 5d. To determine the composition of the synthesized nanotubes, an EDS spectrum was recorded and is presented in Figure 6c. Ti and O are observed with an estimated atomic ratio of 1:2.

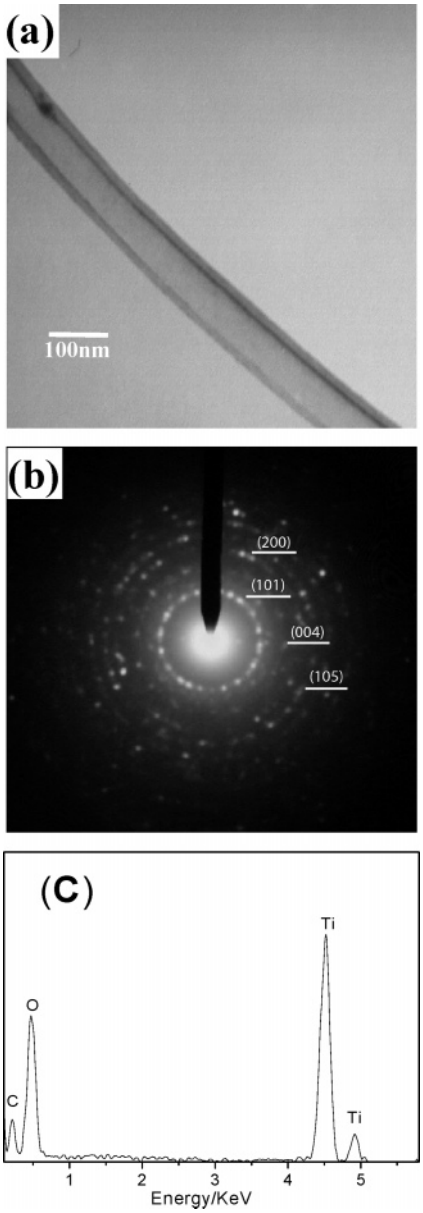

Figure 6. (a) TEM image of a TiO_2 nanotube; (b) SAED pattern of TiO_2 nanotube; and (c) EDS spectrum of the TiO_2 nanotube.

In addition to the Ti and O peaks, a strong C peak is also observed in the EDS spectrum; however, the EDS result cannot distinguish the origin of the C signal, which may arise from carbon doped into the TiO_2 nanotubes and/or carbon on the surface.

Optical Properties and Photocurrent of TiO_2 Nanospheres and Nanotubes. To determine whether carbon was doped into the TiO_2 microspheres and nanotubes and, if so, the effect of carbon doping on their UV−vis light response, we further studied the synthesized TiO_2 structures using UV−vis spectroscopy. The UV−vis spectra of synthesized TiO_2 microspheres and nanotubes are shown in Figure 7. For comparison, the UV−vis spectra of a blank porous alumina template (a) and P-25 film (b) are also included in Figure 7. Comparison of spectrum b (P-25), spectrum c (TiO_2 spheres), and spectrum d (TiO_2 nanotubes) reveals a significant red shift of the absorption edge toward the visible region for both TiO_2 spheres and nanotubes. The absorption

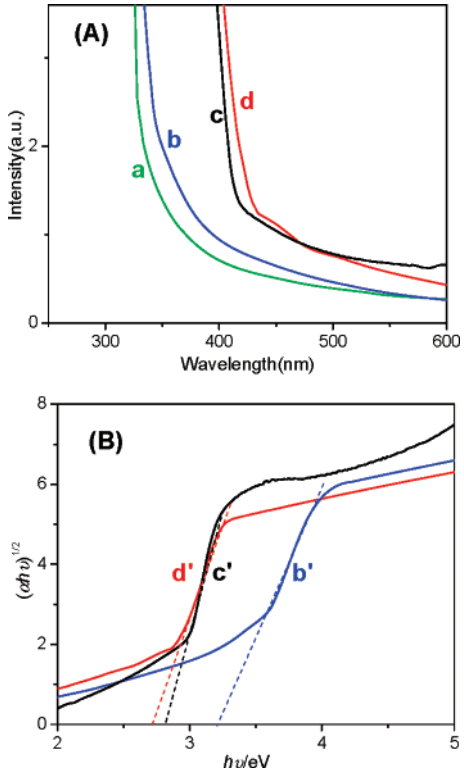

Figure 7. (A): UV−vis spectra of (a) the blank porous alumina template; (b) the P-25 film on the porous alumina template; (c) nanospheres; and (d) TiO_2 embedded in a porous alumina template. (B): Variation of $(\alpha h\nu)^{1/2}$ vs excitation energy ($h\nu$) for the TiO_2 nanosphere and nanotubes to identify indirect transitions: (b′) the P-25 film; (c′) TiO_2 nanospheres; and (d′) TiO_2 embedded in a porous alumina template.

coefficient α and the indirect band gap E_g are related through the following equation[45]

$$(\alpha h\nu)^{1/2} \propto h\nu - E_g \qquad (1)$$

where ν is the frequency, and h is Planck's constant. The Tauc plots, $(\alpha h\nu)^{1/2}$ vs $h\nu$, obtained after substituting the value of α in eq 1, are shown in Figure 7B. The optical band gap, estimated by dropping a line from the maximum slope of the curve to the x-axis, is 2.78 eV for the TiO_2 microspheres and 2.72 eV for the TiO_2 nanotubes, which are much smaller than that of bulk anatase TiO_2 (3.20 eV), indicating that carbon is doped into the TiO_2 crystal lattice. This is consistent with our EDS data: the percentage of carbon in TiO_2 nanotubes is approximately 5%, which is higher than the percentage of carbon in the TiO_2 microspheres (~3%). To further prove that carbon has been doped into TiO_2, not just covering the surface, we did control experiments. Carbon was coated on the surface of P-25 film for 1 min using an EDWARDS coating system. The UV spectrum of the carbon coated P-25 is almost identical to the spectrum of P-25 without coated carbon; thus there is no obvious absorption edge shift when the carbon is simply coated on the surface. All the above results demonstrate that the significant absorption shift shown in Figure 7 is not due to carbon on the surface of the samples; it can thus be ascribed to carbon doped into the TiO_2 microspheres and nanotubes.

(45) Tauc, J. *Mater. Res. Bull.* **1970**, *5*, 721.

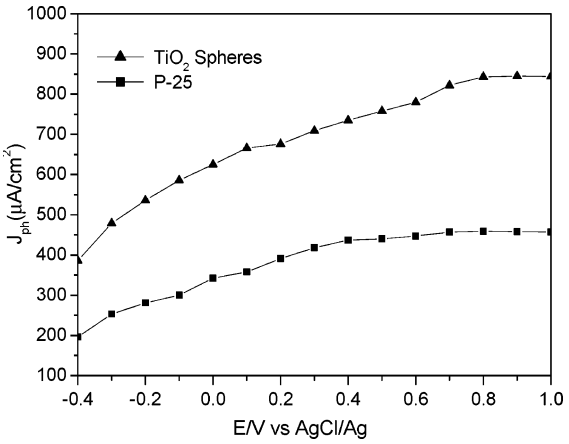

Figure 8. Variation of photocurrent density vs applied electrode potential for the carbon-doped TiO_2 spheres and P-25 film in 0.5 M Na_2SO_4 electrolyte under Hg lamp irradiation (~2 mW/cm^2).

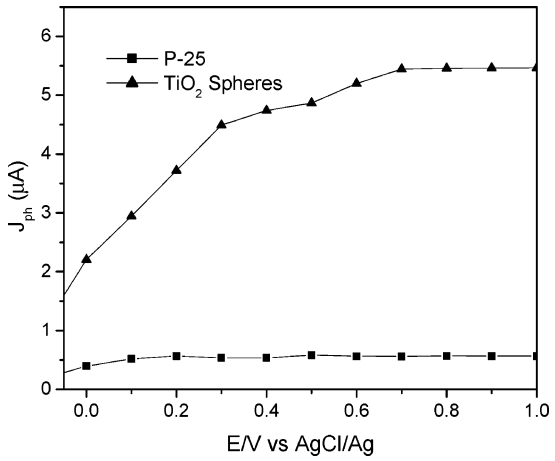

Figure 9. Variation of photocurrent density vs applied electrode potential for the carbon-doped TiO_2 spheres and P-25 film in 0.5 M Na_2SO_4 electrolyte under visible light irradiation (λ>420 nm).

The direct growth of large amounts of TiO_2 spheres on titanium substrates allows us to further study their photoelectrochemical activity. Figure 8 shows a comparison of the photocurrent density vs applied potential curves for the TiO_2 microspheres and one P-25 film under Hg lamp irradiation (~2 mW/cm^2). The electrolyte used in the photoelectrochemical study was 0.5 M Na_2SO_4. The reaction being investigated here is thus the water splitting reaction:

$$2H_2O \rightarrow 2H_2 + O_2 \qquad (2)$$

The photocurrent increases with the increase of the applied electrode potential as the applied positive electrode potential reduces the recombination of the photogenerated electrons and holes. This is consistent with the previous literature results.[14] The photocurrent of the carbon-doped TiO_2 microspheres is approximately 2 times higher than that of the P-25 film showing that the formed TiO_2 microspheres have a much higher real surface area although their geometric surface area is the same.

As seen in Figure 7A,B, the synthesized carbon-doped TiO_2 spheres show enhanced visible light absorption. We further measured the photocurrents of the carbon-doped TiO_2 spheres and the P-25 film under visible light radiation with a wavelength of λ > 420 nm and intensity equal to 0.015 mW/cm^2. As shown in Figure 9, as expected, the photocurrent of P-25 is very low and does not change with increased applied potential. Interestingly, the synthesized carbon-doped TiO_2 spheres show much higher photocurrent than the P-25 film, demonstrating that the carbon-doped TiO_2 spheres can more effectively harvest visible light. This is consistent with the UV−vis results shown in Figure 7.

Growth Mechanisms of the Carbon-Doped TiO_2 Spheres and Nanotubes. The boiling point of the organic Ti precursor $Ti(OC_4H_9)_4$ used in this study is 312 °C. We carried out the same experiment as described in the Experimental Section but at a low temperature (312 °C); very few particles were formed, showing that $Ti(OBu)_4$ is stable and does not decompose at its boiling point. It is expected that several steps are involved in the formation of the carbon-doped TiO_2 spheres: (i) the organic Ti precursor turns to vapor; (ii) the organic Ti vapor passes through the high-temperature zone by diffusion and the push of the carrier gas argon; and (iii) the vapor is decomposed in the high-temperature zone. In a vapor or liquid process via pyrolysis of metallorganic precursors, the decomposition of the reactant is rapid, and the nucleation and growth of TiO_2 particles occur in a quasi-equilibrium state after the completion of chemical reactions. During this process, TiO_2 monomers are formed, and then TiO_2 monomers condensate to form larger clusters by homogeneous nucleation in the gas phase based on the collision mechanism,[46] forming microspheres and nanospheres. Thus, the density of the vapor of the organic Ti precursor has a significant impact on the diameter of the formed TiO_2 spheres. If the density of the vapor of organic Ti compounds is low, the possibility of agglomeration of small TiO_2 droplets reduces greatly, favoring the formation of nanospheres. By changing the flow rate of the carrier gas, one can change the density of the vapor. This is why the diameter of TiO_2 spheres decreased from 2 μm to 100 nm when the flow rate of the carrier gas was increased from 100 to 200 sccm as shown in Figure 3.

Similarly, the formation of the C-doped TiO_2 nanotubes also involves several steps. During the heating process, the organic Ti precursor vaporizes. The evaporated organic Ti molecules enter the porous alumina template and deposit on the inner wall of the nanochannels forming an organic compound layer. The organic layer is then decomposed at the high temperature, forming the TiO_2 nanotubes. It should be noted that the TiO_2 nanotubes can only be synthesized under an inert atmosphere. We also tried the experiments in air, and under an atmosphere purged by oxygen, TiO_2 particles rather than TiO_2 nanotubes were formed in both cases. As thermal decomposition occurs under an inert atmosphere (argon gas), in the absence of O_2, the organic Ti precursor provides both Ti and O sources for the formation of TiO_2 nanotubes. Thus, it is expected that carbon will be easily doped into the TiO_2 in the course of the formation of the TiO_2 spheres and nanotubes. This is why a strong carbon peak appears in the EDS spectrum (Figure 6b) although the sample was annealed in air at 500 °C for 1 h.

(46) Pratsinis, S. E.; Vemury, S. *Powder Technol.* **1996**, *88*, 267.

There are three possible ways to dope carbon into titania: (i) doped carbon as cation replacing Ti; (ii) as anion substituting O; and (iii) insertion of carbon, in anion or cation form, into crystal lattice. To understand how carbon is doped into TiO_2, we did further quantum chemical calculations on the electronic states of anatase titania crystal with doped carbon; details are described in the Supporting Information. Doping of carbon as a tetravalent cation does not influence the CB and VB of pure anatase but induces an interband gap vacant electronic state, which is located above VB by 1.08 eV. Therefore, the results suggest that a new absorption peak at 1.08 eV may appear in the absorption spectrum, and a shift of band edge would not be supported. This is not reflected in our experimental results. Even assuming that carbon is included as anions substituting O, again no band gap narrowing is observed, and an interband gap vacant state appears above VB by 0.46 eV. These results indicate that both cation and anion doping do not account for the present visible-light absorption. Thus, one possible structure of doping is insertion of carbon, in anion or cation form, into crystal lattice. This is consistent with the previous study by Barborini et al.[47] When annealing TiO_2 up to 800 °C, the optical gap remained above 3 eV; but at 900 °C, it suddenly dropped below 3 eV, indicating that carbon diffusion and doping were taking place. The subsequent step at 1000 °C further reduced the gap to the value of 2.06 eV.

(47) Barborini, E.; Conti, A. M.; Kholmanov, I.; Piseri, P.; Podesta, A.; Milani, P.; Cepek, C.; Sakho, O.; Macovez, R.; Sancrotti, M. *Adv. Mater*. **2005**, *17*, 1842.

Conclusions

In summary, we have developed a facile and reproducible method to synthesize, on a large scale, carbon-doped TiO_2 spheres and nanotubes, where the Ti, O, and C are from a single Ti precursor $Ti(OC_4H_9)_4$. The diameter of the spheres can be easily varied from 100 nm to several micrometers by adjusting the flow rate of the carrier gas. The synthesized carbon-doped TiO_2 microspheres and nanotubes possess high photocatalytic activity and enhanced visible light response. The photocurrent of the carbon-doped TiO_2 spheres is much higher than that of P-25, especially under visible light irradiation. Quantum calculations indicate that the possible structure of doping is insertion of carbon into TiO_2 crystal lattice. As the substrate has very little impact on the process of the TiO_2 formation, different carbon-doped TiO_2 nanostuctures can be achieved using different templates. The approach described in this study can also be adopted to fabricate other oxide nanostructures.

Acknowledgment. This work was supported by a Discovery Grant from the Natural Sciences and Engineering Research Council of Canada (NSERC). A. Chen acknowledges NSERC and the Canada Foundation of Innovation (CFI) for a Canada Research Chair Award.

Supporting Information Available: Quantum calculation on the electronic states in anatase titania crystal with doped carbon. This material is available free of charge via the Internet at http://pubs.acs.org.

CM071244M